

# Homoclinic Structure Controls Chaotic Tunnelling

Stephen C. Creagh<sup>a,b†</sup> and Niall D. Whelan<sup>a,c</sup>

<sup>a</sup>*Division de Physique Théorique*<sup>\*</sup>, Institut de Physique Nucléaire 91406, Orsay CEDEX, France.

<sup>b</sup>*Service de Physique Théorique, CEA/Saclay, 91191, Gif-sur-Yvette CEDEX, France.*

<sup>c</sup>*Department of Physics and Astronomy, McMaster University, Hamilton, Ontario, Canada L8S 4M1.*

(December 2, 2024)

Tunnelling from a chaotic well is governed by an infinite set of complex periodic orbits which contain information about both the real dynamics inside the well and complex dynamics under the confining barrier. This intuitive idea is given a precise semiclassical formulation in terms of the homoclinic structure associated with a real trajectory which is smoothly connected to an optimal complex tunnelling path. This theory is verified by considering a model double well problem.

PACS numbers: 03.65.Sq, 73.40Gk, 05.45.+b, 0.320.+i

Tunnelling rates from potential wells with chaotic classical dynamics exhibit strong state to state fluctuations about a mean rate [1]. Such fluctuations appear almost random, and indeed can be fitted to standard distributions of random matrix theory [2]. Nevertheless, we show that there is a simple underlying structure which explains the tunnelling-rate fluctuations in terms of a set of homoclinic orbits. Homoclinic orbits have been recognized to play an important semiclassical role in two different contexts: quantisation using the trace formula [3] and wavepacket recurrences [4]. The present manifestation is new, though a connection will be made with [4].

A typical application of the theory would be for a double well potential  $V(-x, y) = V(x, y)$ , in which we are interested in the spectrum of energy level splittings  $\Delta E_n$  of quasi-degenerate doublets labelled by  $n$ . (We stress, however, that metastable wells can be treated similarly by replacing splittings with resonance widths in what follows [5,6].) It will prove useful, however, to generalise somewhat by considering spectra that depend on a parameter  $q$  and ask for the values  $q_n$  for which a given energy  $E$  is an eigenvalue. (In particular, the choice  $q = 1/\hbar$  [5] will lead to calculations with a fixed classical dynamics throughout the spectrum while in [1] we used  $E$  in place of  $q$ .) In the case of a symmetric double well we can assume approximately degenerate doublets at parameter values  $q_n$  with splittings  $\Delta q_n$  between them. To investigate tunnelling fluctuations we consider the function [1]

$$f(q) = \sum \Delta q_n \delta(q - q_n). \quad (1)$$

On changing the choice of parameter  $q$ , Jacobians cancel and  $f$  remains invariant to leading order in  $\Delta q_n$ . Detailed numerical calculation will be for  $V(x, y) = (x^2 - 1)^4 + x^2 y^2 + \mu y^2$  with  $\mu = 1/10$ .

The spectrum and associated tunnelling rates are encoded in  $f(q)$ . Semiclassically, it can be approximated as a sum over orbits which start on one side of the energy barrier and, after time evolution along a contour in the complex plane, finish at the symmetric image of the initial point on the other side. We will refer to such orbits as being *pseudoperiodic*. In [1] it was shown that

when the optimal tunnelling route is along a symmetry axis, a coherent quasi-periodic oscillation arises in the tunnelling rate that can be related to the action of a real periodic orbit, also on the symmetry axis. However, there remains additional significant fluctuations which we will explain using orbits which are homoclinic to this real orbit. These orbits are not constrained to the symmetry axis and to describe how they contribute, it is convenient to develop an alternate semiclassical interpretation of  $f(q)$ , in terms of a sequence of complex symplectic maps. Construct a surface of section  $\Sigma$  through one of the wells, for example,  $x = x_0$ ,  $H = E$  and  $\dot{x} < 0$ . Denote by  $F : \Sigma \rightarrow \Sigma$  the first-return surface-of-section mapping. According to [7], one can construct within semiclassical calculation a finite-dimensional Hilbert space  $\mathcal{H}$  and a unitary operator  $T$  acting upon it such that  $\Sigma$  and  $F$  are their respective classical limits. When an eigenfunction  $\psi_n(y)$  of  $T$  has eigenphase  $e^{i\theta_n} = 1$ , the corresponding value of  $E$  is an approximate eigenvalue of the Schrödinger operator. In the case of a double well, such a value would approximate the mean position of a doublet.

We include tunnelling [5] by also defining a *complex* symplectic map  $\mathcal{F} : \Sigma \rightarrow \Sigma$ . Note that any potential barrier has an orbit  $\gamma_0$  which crosses it with minimum imaginary action in an imaginary time  $-i\tau_0$ . Though complex throughout most of its evolution, this orbit has turning points at either end where its coordinates in phase space are real. There is a real phase space point  $p_0$  on  $\Sigma$  which evolves to one of these endpoints under real time evolution. It has a symmetric image  $\sigma p_0$  on  $\sigma \Sigma$  which evolves to the other endpoint. (Here  $\sigma$  refers to the symmetry operation — reflection in  $x$  in our example.) The point  $p_0$  evolves into  $\sigma p_0$  if we integrate along a complex time contour  $C$  as follows: first the contour evolves along the real axis until the trajectory reaches the turning point of  $\gamma_0$ , then it descends parallel to the imaginary axis until the turning point on the other side of the barrier is reached and finally retraces the evolution parallel to the real axis (in negative real time) until  $\sigma p_0$  is reached, resulting in a net time of evolution  $-i\tau_0$ . If a neighbouring point  $p'$  of  $p_0$  is chosen on  $\Sigma$ , a deformation of  $C$  can be found

such that the final point  $p$  is on  $\sigma\Sigma$ . We then invoke the symmetry operation to map  $\sigma\Sigma$  back to  $\Sigma$ , thereby defining a complex symplectic map  $\mathcal{F}$  mapping  $\Sigma$  onto itself. Specifically, it is the product of the complex time integration along  $C$  and the mapping by  $\sigma$ :  $\mathcal{F}p' = \sigma p$ . The central orbit  $\gamma_0$  corresponds to a real fixed point  $p_0$  of  $\mathcal{F}$  while other initial conditions, even if real, are mapped to complex images under  $\mathcal{F}$ . Using coordinates  $(y, p_y)$  on  $\Sigma$ , the real action  $S(y, y', E)$  of orbits defining the first return map can be used to construct a semiclassical approximation for the transfer operator  $T$  [7]. Similarly, the deformations of the orbit  $\gamma_0$  that define  $\mathcal{F}$  produce a complex action, which we denote by  $-iK(y, y', E)$ , which can be used to construct a complex operator  $\mathcal{T}$  [5]. (Unlike  $T$ ,  $\mathcal{T}$  is not unitary but hermitian.)

The function  $f(q)$  can then be written as

$$f(q) = \frac{1}{\pi} \sum_{m=-\infty}^{\infty} \text{Tr } \mathcal{T} T^m \quad (2)$$

$$= \frac{1}{\pi} \text{Tr } \mathcal{T} + \sum_{r=1}^{\infty} \frac{2}{\pi} \text{Re } \text{Tr } \mathcal{T} T^r \quad (3)$$

$$\equiv f_0(q) + \sum_{r=1}^{\infty} f_r(q) \quad (4)$$

Before justifying this, let us first interpret it. The trace of the operator  $\mathcal{T} T^m$  is given by the standard semiclassical trace formula as a sum over the fixed points of the corresponding symplectic map  $\mathcal{F} F^m$  [8]. The novel element here is that these maps, along with most of their fixed points, are complex. In the second and third lines we have isolated the  $m = 0$  term, denoted by  $f_0(q)$ , and used the relation  $\text{Tr } \mathcal{T} T^{-m} = [\text{Tr } \mathcal{T} T^m]^*$  (a consequence of the unitarity of  $T$  and the hermiticity of  $\mathcal{T}$ ) and introduced a positive repetition index  $r$ . As discussed in [1],  $f_0(q)$  is determined by the purely imaginary action of  $\gamma_0$ , is monotonic and gives the average behaviour of the splittings. The terms with  $r > 1$  correspond to orbits with real parts to the actions and give fluctuations about this mean. To justify Eq. (2), we note that a formal expression  $\Delta q_n \propto \langle \psi_n | \mathcal{T} | \psi_n \rangle$  is derived in [5] relating the size of an individual splitting to the behaviour of the wavefunction around  $p_0$ . The function  $\sum_n \langle \psi_n | \mathcal{T} | \psi_n \rangle \delta(\theta - \theta_n)$  can then straightforwardly be related to a sum over traces of powers  $\mathcal{T} T^r$  using standard calculation. Taking into account the Jacobian relating  $\theta_n$  to  $q_n$ , Eq. (2) follows.

In problems with an additional symmetry axis (for us it is along  $y = 0$ ), the point  $p_0$  is a fixed point of both  $\mathcal{F}$  and  $F$  and thus of each  $\mathcal{F} F^m$ . The treatment in [1] consisted of treating only this fixed point in each of the terms in (4). We now systematically include the other fixed points, which are generally complex. To do this we note that in the vicinity of  $p_0$ , we can deform real fixed points of the real map  $F^r$  into complex fixed points of  $\mathcal{F} F^r$ ; this is because  $\mathcal{F}$  can be deformed continuously to

the identity map near  $p_0$ . This homotopy between the two classes of orbit is of great help both in the practical task of finding the complex fixed points of  $\mathcal{F} F^r$  and in using them to compute the traces in (3) (determining phases using Maslov indices *etc.*).

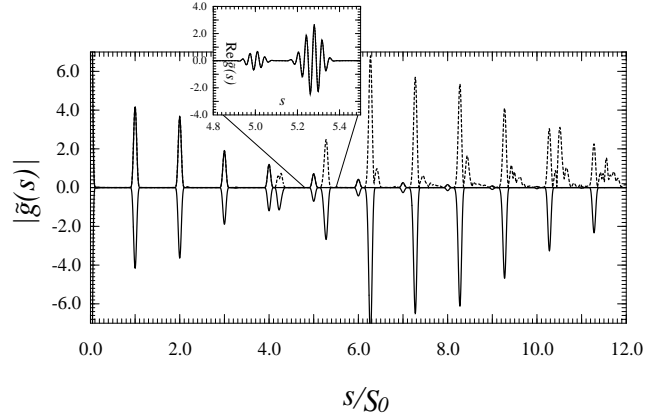


FIG. 1. The upper dashed curve is the Fourier transform of  $g(q)$  obtained quantum mechanically. The upper continuous curve is the semiclassical prediction using just the axial orbits. The lower continuous curve is a result of the theory using the six homoclinic families illustrated in the next figure. The inset compares the quantum-mechanical  $\text{Re } \tilde{g}(s)$  with the semiclassical prediction for the first significant homoclinic cluster.

We now choose the spectral parameter to be  $q = 1/\hbar$  and define the rescaled function  $g(q) = f(q)/f_0(q)$ . This rescaling removes the strong secular variation in magnitude as a function of  $q$ . The trace formula allows us to write  $g(q)$  as the sum

$$g(q) = 1 + \text{Re} \sum_{r=1}^{\infty} \sum_{\gamma \in P_r} A_{\gamma} e^{iq(S_{\gamma} - iK_0)} \quad (5)$$

where  $P_r$  denotes the set of fixed points of  $\mathcal{F} F^r$ . In particular,  $q$  only appears in the exponents. The amplitude  $A_{\gamma}$  is determined by the linearisation of the maps  $\mathcal{F} F^r$  and  $\mathcal{F}$  about  $\gamma$  [1].

In Fig. 1 we show the Fourier transform  $\tilde{g}(s)$  of  $g(q)$  for energy  $E = 0.9$  and  $q$  in the window  $[30, 100]$  (the range  $[0, 30]$  is excluded so as to put us comfortably in the semiclassical regime). For each  $r$ , the fixed point of  $\mathcal{F} F^r$  defined by  $p_0$  has the action  $S_{\gamma} = rS_0 + iK_0$ , where  $S_0$  is the action of the on axis real periodic orbit in one of the wells. Therefore  $\tilde{g}(s)$  exhibits a series of simple peaks at the harmonics  $s = rS_0$  which is well reproduced by the corresponding semiclassical theory. More interesting, however, is the additional structure, primarily in the form of a sequence of regularly spaced peaks shifted away from the simple harmonics which we now explain using nonaxial orbits.

Among barrier-crossing orbits, the minimum imaginary action is that of  $\gamma_0$ ; the contributions of other orbits are exponentially suppressed by order  $\exp(-\Delta K/\hbar)$

where  $\Delta K$  is the additional imaginary action. To be numerically significant, therefore, we are led to consider orbits which minimise this quantity. An obvious choice is the set of orbits that are homoclinic to  $p_0$ . These trajectories, easily calculated from the intersection of stable and unstable manifolds of  $p_0$ , approach  $p_0$  exponentially fast in both forward and backward time evolution — their distance  $d(t)$  from  $p_0$  scales as  $d(t) \sim e^{-\nu|t|}$  as  $t \rightarrow \pm\infty$ , where  $\nu$  is the Liaponov exponent of the real map  $F$  at  $p_0$  and  $t$  is a discrete time. Let  $(\cdots x_{-2}, x_{-1}, x_0, x_1, x_2 \cdots)$  be the intersection of one such trajectory with  $\Sigma$ . Then, a truncation  $(x_{-M} \cdots x_{-1}, x_0, x_1, \cdots, x_N)$  is a finite length trajectory which is almost a periodic orbit if  $M$  and  $N$  are large because  $x_{-M}$  and  $x_N$  are close to each other and to  $p_0$ . By slightly perturbing the initial condition, one can find a nearby fixed point of  $F^{r+1}$  (a real periodic orbit) or a fixed point of  $\mathcal{FF}^r$  (a complex periodic orbit), where  $r = M + N$ . In the latter case, the tunnelling segment of the trajectory is very close to  $\gamma_0$  and as a result the imaginary part of the action is close to the optimal value  $K_0$ . In the trace formula, there is then a competition of exponentials — the imaginary part of the action will decay exponentially with length according to  $\text{Im}(S_\gamma - iK_0) \sim e^{-\nu \min(M, N)}$  and this can be smaller than  $\hbar$  so that  $e^{-q(S_\gamma - iK_0)}$  is nonnegligible.

The equal spacing of the peaks is easily explained in this scenario. Allowing an orbit with one extra iteration of the real map (corresponding to the truncation  $(x_{-M} \cdots x_{-1}, x_0, x_1, \cdots, x_{N+1})$  for example) amounts to including an extra  $F$ -bounce near  $p_0$ , which, to a good approximation, adds  $S_0$  to the action. It also explains why the peaks are so much larger than the simple peaks at  $s = rS_0$ , beyond about  $r = 5$ . Each homoclinic peak actually contains the contribution of many fixed points, all with approximately the same action. This quasidegeneracy is both because there is more than one homoclinic trajectory and because any given homoclinic trajectory has many truncations of a given length, corresponding to different choices of  $M$  (the effective number depends on  $q$  and is limited by the criterion that  $\text{Im}(S_\gamma - iK_0) \sim e^{-\nu \min(M, N)} \lesssim \hbar$ ). The amplitude of any single orbit decays exponentially with length due to it being increasingly unstable but this is initially overcome by the increasing quasidegeneracy — hence the rising peak-height until  $r = 7$ . The exponential decay eventually triumphs over the algebraically growing quasidegeneracy so there is a subsequent fall. As this happens, additional side-peaks appear, which we ascribe to secondary homoclinic intersections. This scenario is reminiscent of the calculation of wavefunction recurrences in [4] where there is also a selection of trajectories which return to a classically small region of phase space, as determined by a Gaussian wavepacket. In our case the selection is through the (near-Gaussian) kernel of  $\mathcal{T}$ . Fourier analysis then reveals peak structure similarly organised around homoclinic orbits [4,9].

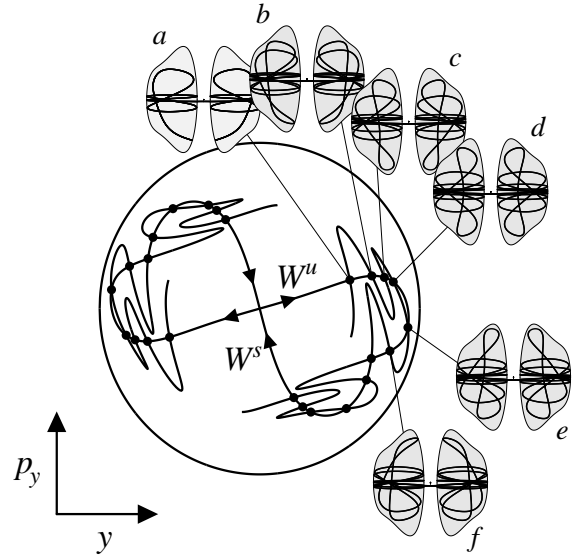


FIG. 2. The surface of section defined by  $E = 0.9$  and  $x = 0.6$ . The circle is the boundary of the energetically allowed region.  $W^u$  and  $W^s$  are the stable and unstable manifolds whose intersections define the homoclinic trajectories: the six distinct ones being labelled  $a$  to  $f$ . For each one, we show the trajectory in configuration space of a corresponding tunnelling periodic orbit.

To explore this structure more explicitly, we examine the classical dynamics in detail for the potential  $V(x, y)$ . Shown in Fig. 2 are the invariant manifolds of  $p_0$  in the surface of section defined by  $x = 0.6$ . Of particular interest to us is a sequence of 6 primary intersections labelled  $a$  to  $f$ . (The other intersections in the figure are either iterates of these six or are related by reflection in  $y$  and  $p_y$ .) Each of these intersections defines a different homoclinic trajectory, and a corresponding series of fixed points of  $\mathcal{FF}^r$ . Also shown in Fig. 2 are the paths in real configuration space of complex trajectories defined for each of these intersections by the truncation  $(M, N) = (3, 5)$  corresponding to the peak at  $s \approx 8.2S_0$ . (Actually shown is a full periodic orbit which is a double iteration of the pseudoperiodic orbit used in calculation. Also, only the real parts are shown; the coordinates also have small imaginary components too small to see.) Each intersection defines a family of such complex trajectories, indexed by  $M$  and  $N$ . The following is an intuitive picture of the differences between members of a family. For sufficiently large  $r$ , we can find a single real periodic orbit near any given intersection (taken from  $\{a, b, c, d, e, f\}$ ). From this orbit, a sequence of complex pseudoperiodic orbits can be constructed as follows. The real orbit, approximating a homoclinic trajectory, will spend a large part of its evolution bouncing back and forth near the on-axis periodic orbit defined by  $p_0$ . At any one of these bounces at the central barrier, we can attach a tunnelling segment of imaginary time evolution. The resulting structure is discontinuous and is not an orbit. However, there is a nearby

pseudoperiodic orbit which can be found numerically by complex Newton iteration. Each choice of bounce results in a different complex orbit, corresponding to a different choice of  $M$  (and  $N = r - M$ ). While the arguments above are asymptotic in  $M$  and  $N$ , we found in practice that complex orbits could usually be found in this manner as long as  $M, N > 2$ .

In addition to the choice of bounce, the symmetries of time-reversal and reflection in  $y$  lead to degeneracy. The families of  $b$  and  $c$  are respectively mapped into those of  $f$  and  $e$  under a combination of the two symmetries. Congruent but distinct families are obtained if we apply either symmetry alone. Both of these families are therefore four-fold degenerate. The family  $a$  maps to itself under time-reversal but a distinct family is obtained under reflection in  $y$ , while the converse applies to  $d$ . We therefore really only have four inequivalent families:  $a, b, c$  and  $d$  with degeneracies of 2, 4, 4 and 2 respectively, for a total of 12. This high degree of degeneracy (including also the choice of bounce) in comparison with the single axial orbit is responsible for the relative dominance of the associated peaks in Fig. 1. In the resolution presently available, the individual contributions of  $\{a, b, c, d\}$  are not resolved, but presumably would be with a wider  $q$ -window. There will always remain a finite resolution for each intersection because of the variation in  $\text{Re } S_\gamma$  as the tunnelling segment is moved further from the center.

To get detailed agreement in Fig. 2 we had to include a family of “ghost” orbits in addition to the orbits described above. Near the intersections  $a$  and  $b$ , there is a switchback in the stable manifold emanating from  $f$  that almost produces two additional intersections; at lower energies these intersections actually occur and lead to two new families of orbits. These can be tracked up to  $E = 0.9$ , although they become complex. (These orbits are analogous to the ghost orbits of [10].) One of them is exponentially large and is excluded through the Stokes phenomenon. The other does contribute and is an important component in the leading edges of the peaks. The Fourier transform is then almost completely reproduced up to about  $s = 8S_0$ . Thereafter additional side peaks emerge which can be similarly explained by secondary intersections (which would be seen in the figure if the invariant manifolds were extended.) Therefore, a systematic calculation of homoclinic structure suffices for a complete understanding of chaotic tunnelling rates.

While the details presented here are limited to systems with additional symmetry in  $y$ , we claim that the guiding principle applies generally. Even if the real extension of  $\gamma_0$  is not periodic, tunnelling rates will be controlled by trajectories homoclinic to it (which are defined in hyperbolic systems even for nonperiodic orbits), although they will not be as simply organised as here. The problem then reduces to an investigation of real chaotic dynamics, after which coupling to the tunnelling part is straightforward. The important physical notion is that homoclinic tra-

jectories are asymptotic to the optimal tunnelling route while fully exploring classical phase space. They therefore contain information about the global dynamics while having a small enough tunnelling action to be significant. This means that they can provide sufficient information to determine the splittings completely, which is something the axial orbits of [1] cannot do.

There has been a lot of recent effort to understand tunnelling in the presence of chaos, often for systems with dynamical rather than energetic barriers, such as KAM surfaces [11,12]. The results are complementary to ours since they typically involve tunnelling from a state associated with a regular part of phase space. It is of interest to understand if there is any connection with the present work. In particular, an exhaustive semiclassical analysis was carried out for one particular system in [12]. The phase space structures which arose appear to be quite distinct from the homoclinic orbits considered here. The development of a more unified picture of these systems certainly deserves exploration.

---

<sup>†</sup> Present address: Division of Theoretical Mechanics, School of Mathematical Sciences, University of Nottingham, NG7 2RD, UK.

<sup>\*</sup> Unité de recherche des Universités de Paris XI et Paris VI associée au CNRS.

- [1] S. C. Creagh and N. D. Whelan, Phys. Rev. Lett. **77**, 4975 (1996).
- [2] S. C. Creagh and N. D. Whelan, to appear.
- [3] A. Ozorio de Almeida, Nonlinearity **2**, 519 (1989).
- [4] S. Tomsovic and E. J. Heller, Phys. Rev. E **47**, 282 (1993).
- [5] S. C. Creagh and N. D. Whelan, chao-dyn/9808014, to appear in Ann. Phys.
- [6] M. W. Beims, V. Konreatovich and J. B. Delos, to appear in Physical Review Letters.
- [7] E. B. Bogomolny, Nonlinearity **5**, 805 (1992).
- [8] M. Tabor, *Chaos and Integrability in Nonlinear Dynamics: An Introduction* (New York, Wiley, 1989).
- [9] K. Hirai and E. J. Heller, Phys. Rev. Lett. **79**, 1249 (1997).
- [10] M. Kus, F. Haake and D. Delande, Phys. Rev. Lett. **71** 2167 (1993).
- [11] W. A. Lin and L. E. Ballentine, Phys. Rev. Lett. **65**, 2927 (1990); O. Bohigas, S. Tomsovic and D. Ullmo, Phys. Rev. Lett. **64**, 1479 (1990); Phys. Rep. **223**, 45 (1993); O. Bohigas et al., Nucl. Phys. A560, 197 (1993); S. Tomsovic and D. Ullmo, Phys. Rev. E **50**, 145 (1994). E. Doron and S. D. Frisch, Phys. Rev. Lett. **75**, 3661 (1995); Phys. Rev. E **57**, 1421 (1998).
- [12] A. Shudo and K. Ikeda, Prog. Theor. Phys. Supplement No. 116, 283 (1994); Phys. Rev. Lett. **74**, 682 (1995); *ibid.* **76**, 4151 (1996); Physica D **115**, 234 (1998).